Self-assembly of tetrathiafulvalene derivatives at a liquid/solid interface—compositional and constitutional influence on supramolecular ordering†

Mohamed M. S. Abdel-Mottaleb‡,§[a] Elba Gomar-Nadal‡,¶[b] Mathieu Surin,[c] Hiroshi Uji-i,[a] Wael Mamdouh,[a] Jaume Veciana,[b] Vincent Lemaur,[c] Concepció Rovira,[b] Jérôme Cornil,[c] Roberto Lazzaroni,[c] David B. Amabilino,*[b] Steven De Feyter*[a] and Frans C. De Schryver[a]

Received 1st July 2005, Accepted 2nd September 2005
First published as an Advance Article on the web 26th September 2005
DOI: 10.1039/b509336h

The self-assembly of a series of tetrathiafulvalene (TTF) derivatives at the interface between non-volatile organic solutions and the graphite surface has been studied by scanning tunnelling microscopy (STM). The TTFs have been prepared such that they bear none, one, two (in different constitutions) or four alkyl chains of different lengths and different functional groups. The STM images reveal that the packing of the TTF cores can effectively be controlled by changing the substitution pattern on the heterocycle. Several structures are seen at the interphase—parquet-type packing, single and double core tapes, and even isolated molecules—all of which have the TTF core essentially coplanar with the surface. Molecular modelling has shown that several orientations of the molecules are practically equal in energy on the graphite, which explains the polymorphous packing of some of the molecules. Solvent effects also play a role in determining the 2D structures.

Introduction

The preparation of organized layers of molecules has found an evocative paradigm in the form of ''self-assembly'',[1] which, it is hoped, will aid in the nanoscale fabrication of more efficient electronic devices.[2] On the one hand, the self-assembly of such layers can be integrated with existing techniques to enable the fabrication of devices on scales unreachable through the exclusive use of current techniques,[3] and therefore can be considered as an extension of the current micro-fabrication techniques into the nano-fabrication domain, through chemistry.[4] On the other hand, organic monolayers can be used in their own right to build specifically functionalized nano-structures that may substitute some electronic components.[5]

Self-assembled monolayers can be divided into two broad classes: chemisorbed and physisorbed. The former, in which molecules are covalently linked to the surface,[6] have been extensively studied and developed.[7] This fabrication approach has been generally used in connection with the current established micro-fabrication techniques.[4,8] In contrast, physisorbed monolayers of small molecules which can be visualized with high-resolution scanning probe microscopes,[9] have not received the same amount of attention in this respect, probably because of the difficulty of controlling the exact location of the adsorbed molecules—among other factors—due to the dynamic nature of the interaction between the molecules and the substrate.[10] The possibility of using self-assembled monolayers to build 2D templates[11] has a potential extension in building specifically functionalized 3D nano-structures. It is the understanding of the molecule–substrate and molecule–molecule interactions that would enable us to overcome the disadvantages of physisorbed monolayers and at the same time enhance our control over the monolayers. One of the main advantages of self-assembly is the possibility of encoding the information for building specific packing patterns on the surface in the chemical structure of the molecules, often by exploiting non-covalent interactions such as hydrogen bonding and coordination bonds, which has been demonstrated by various experimental STM[12] and AFM[13] results. In addition to varying the nature and position of functional groups in the molecules, the two-dimensional ordering is often affected by the number and length of alkyl chains,[14] which is explained in terms of the competition between interactions driven either by the alkyl chains or the functional groups present in the molecules. Thus, alkyl chain number and length is one possible way of controlling the packing pattern of the molecules in the monolayer. Ultimately, if the functional moieties in the molecule are electronically

[a]*Laboratory of Photochemistry and Spectroscopy, Molecular and Nano Materials, Department of Chemistry, Katholieke Universiteit Leuven (KULeuven), Celestijnenlaan 200-F, 3001 Leuven, Belgium. E-mail: steven.defeyter@chem.kuleuven.be; Fax: +32 16 32 79 90; Tel: +32 16 32 79 21*
[b]*Institut de Ciència de Materials de Barcelona (CSIC), Campus Universitari de Bellaterra, 08193 Cerdanyola del Vallès, Catalonia, Spain. E-mail: amabilino@icmab.es; Fax: 34 93 5805729; Tel: 34 93 580 1853*
[c]*Service de Chimie des Matériaux Nouveaux, Université de Mons-Hainaut, 20, Place du Parc, B-7000 Mons, Belgium*
† Electronic supplementary information (ESI) available: synthetic and spectroscopic details of the TTF derivatives. See DOI: 10.1039/b509336h
‡ These authors contributed equally to the work described in this paper.
§ Current address: Department of Optical Spectroscopy and Molecular Physics, Institute of Physics, Chemnitz University of Technology, Reichenhainerstr. 70, D 09107 Chemnitz, Germany.
¶ Current address: Materials Research Science and Engineering Centre, 2120 Physics Building, University of Maryland, College Park, MD 20742-4111, USA.

interesting, using the substitution pattern of the alkyl chains and their different length would enable control over the position and orientation of such moieties on a surface.

In this context we are studying the self-assembly of a number of tetrathiafulvalene derivatives (TTFs) at a liquid/solid interface. TTFs are ideal candidates for possible applications in molecular electronics, since they undergo two reversible one-electron oxidation steps at well-defined redox potentials to form the corresponding radical cations and di-cations and they have an extremely rich supramolecular chemistry.[15] In addition, the radical cations of TTFs have been successfully employed as components in electrically conducting and superconducting salts and charge-transfer complexes,[16] and the neutral components have shown high transport mobility in field effect transistors.[17] While the charge transfer complex TTF–tetracyanoquinodimethane (TCNQ) and related salts have been studied by STM extensively,[18] molecular level information on the neutral donors in general is lacking. For the self-assembly of neutral TTF derivatives at surfaces, it is interesting to know the dominant non-covalent forces that determine the organisation.[19,20] Although the supramolecular chemistry of TTFs in crystals is established (π–π stacking and S···S side-on interactions dominate)[21] the way the molecules interact between each other at surfaces is not known with certainty. From the 'molecular electronics' point of view, it is important to control the organisation of monolayers and films of TTFs.[22] The question arises, can the intermolecular interactions be used to influence packing in two dimensions? The presence of the substrate and the substitution pattern of the molecules will play decisive roles in the intermolecular interactions and two-dimensional patterns formed.

We report here an STM investigation of the 2D organization at a liquid/graphite interface of the series of neutral TTF derivatives shown in Chart 1, along with the syntheses of these compounds. Included in the molecules we selected within this series are TTFs with none, one, two (in different orientations), and four alkyl chains of differing lengths attached to the π-electron rich core. It was envisaged that these alkyl chains would assist in anchoring the molecule to the surface through van der Waals interactions with graphite.[23] Also present are molecules that can interact through hydrogen bonds. We will demonstrate how these different molecular features influence the packing of the resulting monolayers.

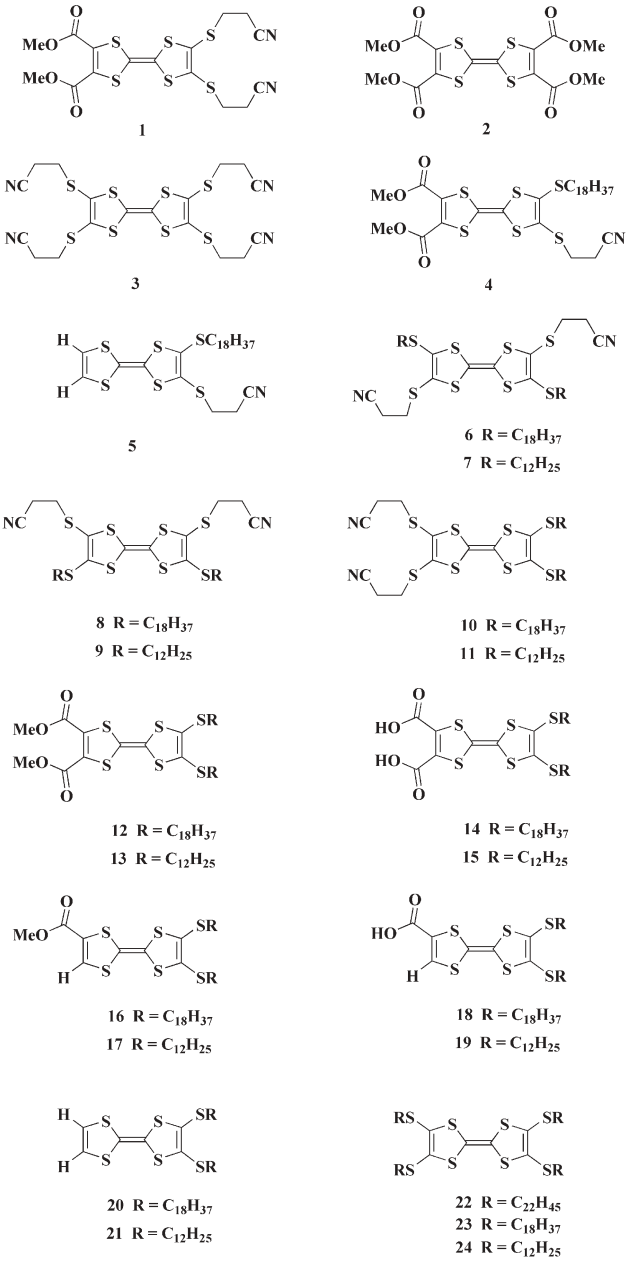

Chart 1

Results and discussion

1. Synthesis

The TTF derivatives **1**, **2**, **3**, **23** and **24** (Chart 1) were prepared according to literature procedures,[24–27] and were purified and characterized as such. Compound **4** incorporating one alkyl chain was prepared according to the route shown in Scheme 1. Starting from the known zinc(II) complex **25**[28] treatment with 3-bromopropionitrile in refluxing acetonitrile gave thione **26** practically quantitatively. Thiones **28** and **29** were prepared by the selective monodeprotection of **26** developed by Becher and colleagues,[24] either by isolation of the cesium salt **27** or through a one pot reaction. In our hands, the latter proved to be more efficient. Coupling of the thione **28** with ketone **32**[29] in refluxing trimethylphosphite afforded compound **4**. Treatment of this compound with LiBr in HMPA to remove the carboxylate groups afforded the TTF derivative **5**.

Compounds **6**–**9** were prepared by coupling the ketones **30** and **31** together using trimethylphosphite. These ketones were prepared from the thiones **28** and **29** by treatment with mercury (II) acetate. The coupling reaction yields a mixture of the *cis* and *trans* isomers **6** and **8** and **7** and **9**, respectively, which were separated by flash column chromatography on silica gel. This kind of separation is not trivial, being achieved normally on account of their different solubility,[30] and care has to be taken to avoid acids which are known to aid the isomerization process.[31] The isomers present different NMR spectra, although they give an identical number of resonances because of their C_{2v} and C_{2h} symmetries, while other spectroscopic characteristics are identical for the two compounds.

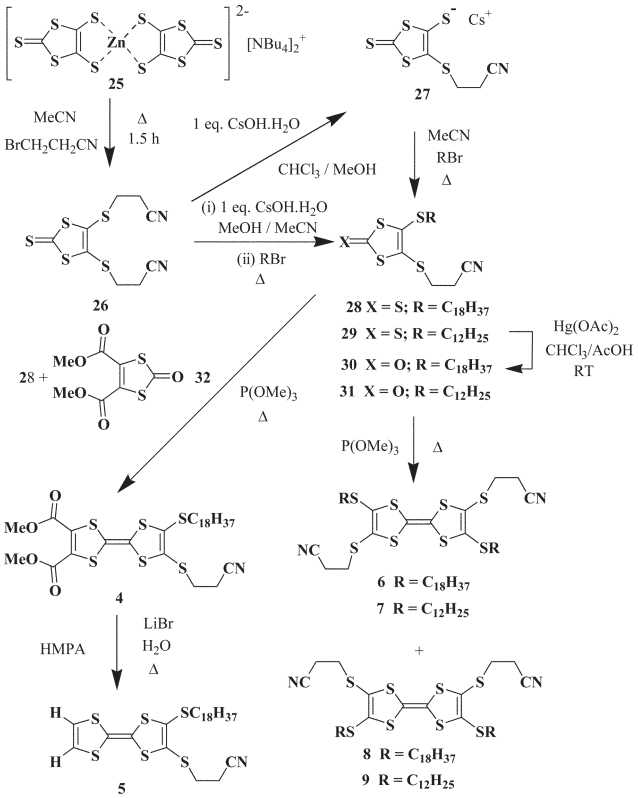

Scheme 1

Their assignment was made based on their polarity, the first-eluted material from the column was therefore supposed to be the *trans* isomer. STM experiments support this assignment.

The constitutional isomers of compounds **6**–**9**, the TTFs **10**[24] and **11**, were prepared (Scheme 2) by the coupling of ketone **33**[26] with the appropriate thione **34** or **35**, respectively.

The known compounds **12**[32] and **13**[33] were mono- and di-decarboxylated to produce **16**, **17**, **20** and **21**, respectively (Scheme 3). The use of LiBr in HMPA at moderately high temperatures (80 °C) leads to selective monodecarboxylation while heating up to 150 °C leads to removal of both groups. Saponification of the ester groups under basic conditions gave the desired mono- and di-carboxylic acid TTF derivatives **18**, **19**, **14** and **15**. Compound **22** was prepared in a manner analogous to **23** and **24**[27] from complex **25**, through alkylation with 1-bromodocosane, conversion of the resulting thione to ketone, and phosphate-mediated coupling.

2. Electrochemistry

The redox properties of the TTF core are influenced strongly by the substituents attached to it,[34] a reflection of the π-electron richness of the system which will, in turn, effect its

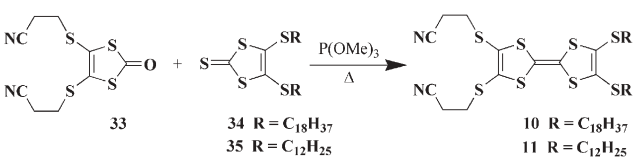

Scheme 2

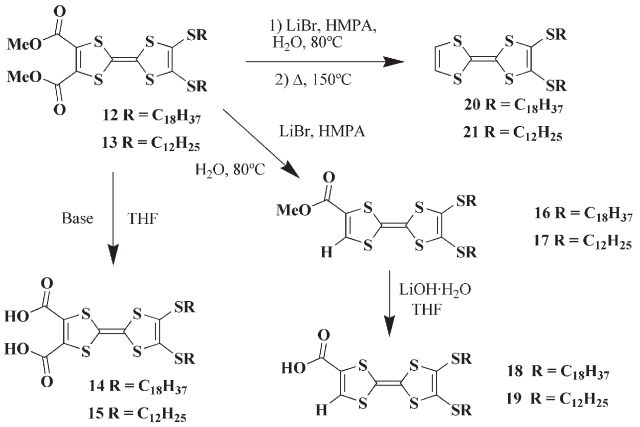

Scheme 3

supramolecular chemistry. The redox potentials of some representative examples of the compounds reported here obtained under standard cyclic voltammetry conditions are given in Table 1.[35] As can be appreciated from these data, the presence of carboxy groups dramatically reduces the donor ability of the molecules, as the first and second one-electron oxidation potentials increase, and the most active donors are those with protons attached directly to the TTF rings.

3. Scanning tunnelling microscopy at the liquid/solid interface

The compounds in Chart 1 were dissolved in 1-octanol or 1-phenyloctane, and a drop of these solutions was deposited on freshly-cleaved graphite. The tip of the STM was immersed in the solution while imaging.[9–12] Thus, the monolayer can be a dynamic system under these conditions, although in general, lateral movement is slow on the timescale of the experiment (typically around 2 min). Below, we compare and contrast the most pertinent results obtained with this series of compounds. In all images white corresponds to high tunnelling current and black to low tunnelling current. The TTF residues always show very high tunnelling current compared with the alkyl chains, although, as shall be seen, the nature of the contrast varies widely.

Non-aliphatic TTF derivatives. TTF derivatives **1**, **2**, and **3** (Chart 1) were investigated at the liquid/solid interface as deposited from 1-octanol or 1-phenyloctane. Only monolayers of the dissymmetric TTF **1**—incorporating ester groups at one "end" and propionitrile groups at the other—were observed, and only at the 1-octanol/graphite interface (Fig. 1). The molecules form a monolayer which appears to have a

Table 1 Examples of oxidation potentials for TTF derivatives described in this paper. Potentials *vs.* Ag/AgCl, Pt working electrode and contact electrode, respectively, in CH_2Cl_2

Compound	$E(0/\cdot+)_{1/2}$/V	$E(\cdot+/2+)_{1/2}$/V
21	0.504	0.976
24	0.568	0.917
17	0.632	1.043
13	0.695	1.040
11	0.650	1.014

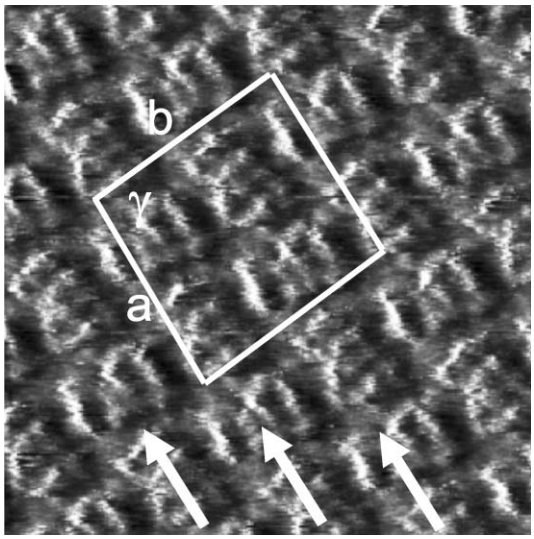

Fig. 1 An STM image of **1** at the 1-octanol/graphite interface. White arrows indicate three tapes. Image size is 5.1 × 5.1 nm. I_t = 2 nA, and V_t = −0.67 V.

parquet-type two-dimensional packing (white arrows) with alternating parallel and perpendicular orientations of contrast with respect to a given direction. The distance between equivalent positions along a given row in the parquet is 27.3 ± 0.2 Å (marked as (a) in Fig. 1). The distance between two equivalent points on abutting rows is 16.5 ± 0.5 Å. (Half of (b), as indicated in Fig. 1). There is no obvious dissymmetry in the images which could be related with the structure of the molecules. The supramolecular chemistry of TTFs in crystals is dominated by π–π stacking and S···S side-on interactions. On the surface of graphite, it seems that the former is suppressed because of the preferential π–π stacking of the TTF moieties with the π system of the substrate. Indeed, TTF derivatives are known to form stacking interactions with graphite-like structures, the fullerenes.[36]

Using either 1-octanol or phenyloctane, monolayers of the symmetric molecules **2** and **3** were not observed at the liquid/solid interface. The electronic character of the π system is very different in the three cases: compound **3** is the more π-electron rich one and compound **2** the more electron poor. The exact reason for the adsorption of **1** and not that of **2** and **3** awaits a clear explanation. Note however that **1** is the only compound within this series of TTF derivatives with a permanent dipole moment.

Monoalkylated TTF derivatives. TTF derivatives **4** and **5** (Chart 1) both incorporate octadecyl chains and differ only in the presence of ester groups or hydrogen atoms at one "end" of the molecule. Despite this apparently minor difference, monolayers of **4** were spontaneously formed (as for structurally-related **1**) upon deposition from either 1-octanol or phenyloctane, but deposition of solutions of **5** in either solvent did not result in monolayers being observed at the liquid/solid interface.

The STM images of a monolayer of **4** in 1-octanol (Fig. 2a) reveal a lamellar structure in which the molecules lie head-to-head, and the alkyl chains from adjacent lamellae interdigitate.

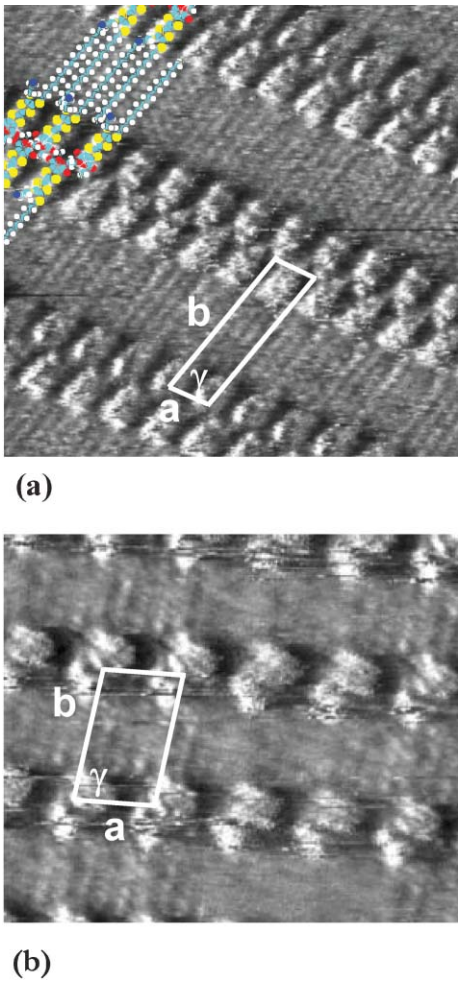

Fig. 2 STM images of the monolayers of **4** at the liquid/solid interface. (a) Deposited from 1-octanol, the lamellar structure is evident, and the alkyl chains interdigitate. Seven model molecules are superimposed on the STM image for clarity. Image size is 11.9 × 11.9 nm; I_t = 0.8 nA; V_t = −0.616 V. (b) Deposited from 1-phenyloctane, image size is 9.1 × 10.6 nm, I_t = 0.5 nA, V_t = −0.46 V.

The distance between two equivalent points in molecules within the lamellae (unit cell parameter *a*) is 13.4 ± 0.2 Å and the distance between identical environments in abutting lamellae (unit cell parameter *b*) is 36.4 ± 1.1 Å. These packing parameters suggest that the cyanoethyl groups and at least one of the ester groups per TTF moiety are not fully adsorbed on the graphite surface. Indeed, the X-ray crystal structure of a 2,3-bis(carboxy)-tetrathiafulvalene shows that the two carboxy groups do not lie parallel to the plane of the TTF ring, and are twisted with respect to it and each other.[24] When physisorbed from phenyloctane (Fig. 2b), the distance between the bright structures along a row is larger than in 1-octanol (a = 19.2 ± 0.2 Å). The other unit cell parameters are b = 35.5 ± 0.5 Å and γ = 85 ± 1. This implies that a bright structure might be composed of more than one TTF molecule as the number of alkyl chains observed on the substrate is higher than the number of bright spots: 2 alkyl chains per bright spot are observed in phenyloctane and in 1-octanol, 3 alkyl chains per 2 bright spots. The difficulties in defining a very precise structure to the monolayer are compounded by the highly variable

contrast exhibited by the TTF cores (*vide infra*), but we can conclude that in both monolayers, the π-electron rich units are oriented side-on and head-to-head in a continuous tape.

Dialkylated TTF derivatives. TTF derivatives **6**–**17** (Chart 1) were investigated at the liquid/solid interface in order to further understand the effect of the substitution type and constitution on the 2D packing pattern. Thus, there are compounds with alkyl chains at the same "end" of the TTF unit (at the 2 and 3 positions) or at opposite "ends" but different "sides" (either 2 and 6 or 2 and 7). The 2D organization of the *trans* compound (**6**) and the *cis* compound (**8**)—which are constitutional isomers—at the liquid/graphite interface has been previously communicated by us,[19] but it is important to discuss more deeply the features of these systems here so that they can be compared with the other compounds.

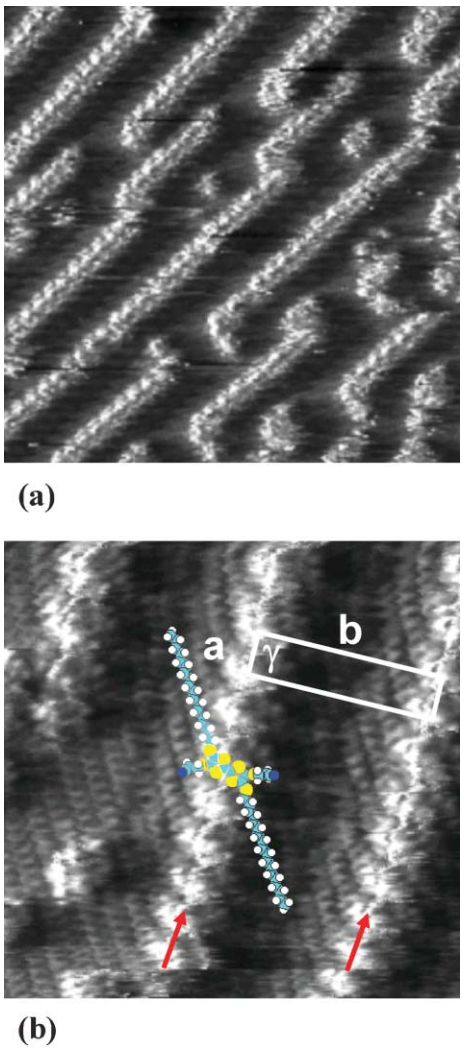

Fig. 3 (a) Large-scale STM image of the monolayer of the *trans*-isomer **6**. Lamellar structure is evident. Image size is 24.9 × 24.9 nm; I_t = 0.5 nA; V_t = −0.63 V. (b) A close-up STM image of the lamellar structure of **6**. Red arrows indicate TTF moieties aligned in the middle of the lamellae. A model molecule is superimposed on the image for clarity. Image size is 10 × 10 nm; I_t = 0.5 nA; V_t = −0.226 V.

Monolayers of the *trans* isomer **6** with octadecyl chains are only formed from 1-octanol. Fig. 3a shows an STM image of an area of one of the monolayers where a tape-like structure can be observed clearly, and in which frequent kink-type defects are present. A closer view (Fig. 3b) reveals submolecular resolution, especially clearly in the alkyl chains. The intermolecular distance between two successive molecules in a lamella, *a*, is 8.3 ± 0.2 Å and the distance between two equivalent points in abutting lamella, *b*, is 36 ± 1 Å, a relatively large separation due to the non-interdigitation of the alkyl chains.

As we suggested above, the contrast of the TTF units is variable as a result of scanning effects. Comparison of the STM images of a *trans*-**6** monolayer recorded at different rotation angles (Fig. 4a–b, defined as the relative angle

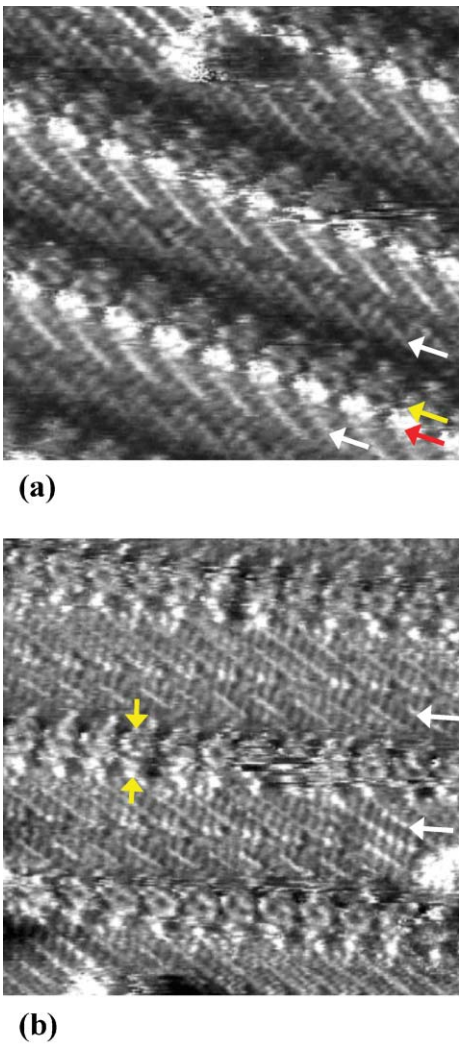

Fig. 4 (a) STM image of monolayer of **6**. Alkyl chains are clearly resolved (white arrows) and the TTF moieties appear with a slightly different contrast (yellow and black arrows). Image size is 9.0 × 9.0 nm; I_t = 0.5 nA; V_t = −0.204 V. (b) STM image of the monolayer of **6** at the liquid/solid interface, again the alkyl chains can be clearly identified (white arrows). The TTF moieties are submolecularly resolved; the two rings of the TTF moieties can be pointed out (yellow arrows). Image size is 11.7 × 11.7 nm. I_t = 0.5 nA; V_t = −0.218 V.

between the lamellae and the scan direction, which is always from left to right in the images) reveals striking differences. In Fig. 4a, the TTF moieties appear as a bright spot (red arrow) with adjacent grey area (yellow arrow). The alkyl chains are well-resolved (white arrows). In Fig. 4b, the TTF moieties appear with yet another contrast, in this case the two rings of the TTF moieties can be pointed out (yellow arrows). The alkyl chains are again well resolved (white arrows). We can see in these images (and it is true for all images recorded) that when the tape axis does not coincide with the scan direction the part of the TTF moiety that the STM tip "hits" first appears brighter than the rest of the same unit. These differences in contrast are thus thought to be due to the change in the scan direction with respect to the adlayers. In all cases, the packing parameters did not change. In the image shown in Fig. 4b, noisy streaks are also apparent where the tip passed over the TTF core, a very common situation in this group of compounds (see also Fig. 6 below). We interpret this effect as a strong interaction between the tip and the core of the molecules under the conditions of the experiment.

Co-existing with this packing (labelled as the α-polymorph) is a second polymorph (β) of *trans*-**6**. Fig. 5a shows an STM image where the two polymorphs are observed simultaneously. In the domains labelled α, the molecules are organized in the lamellar packing discussed above, while the β polymorph, has an alternating double-core–single-core lamellar structure (red and yellow arrows, respectively). It is interesting to note the strict adherence to this packing pattern. Even the presence of defects does not interrupt the continuation of the structure. Fig. 5b is a zoom-in on the area indicated in Fig. 5a. In this STM image, two double-core lamellae (red arrows) and a single-core lamella (yellow arrow) can be observed. The intermolecular distance between two equivalent points in a lamella is $a = 15.2 \pm 0.9$ Å and the distance between corresponding points on two equivalent lamellae is $b = 84 \pm 2$ Å. The intermolecular distance did not change (within the experimental error) for molecules adsorbed in a double-core or single-core lamella. The alternation between double and single rows can be explained as a result of the constraints imposed by the alkyl chain interactions in order to form a dense 2D packing with optimized van der Waals interactions between the alkyl chains and between them and the surface. Monolayers of the *trans*-isomer **7**, which differs from **6** in the length of the alkyl chain (12 versus 18 carbon atoms), were not observed in either solvent in several sessions.

The *cis*-isomer **8** forms monolayers spontaneously at the liquid/solid interface in either 1-octanol or 1-phenyloctane. Fig. 6a shows a large-scale image of such a monolayer in which a lamellar structure is evident. The image is again submolecularly resolved, allowing the identification of the different parts of the molecule. The TTF cores appear with a bright contrast while the octadecyl chains appear with a darker contrast. The alkyl chains are perpendicular to the lamellar axis and interdigitate. No single-core lamellae of **8** were observed in any of the many imaging sessions. The distance between two equivalent molecules in a lamella is $a = 17.8 \pm 0.9$ Å and the distance between two equivalent points in abutting lamellae is $b = 34.6 \pm 1.5$ Å. Fig. 6b shows a close-up STM image of the monolayer of **8**, where the cores and the alkyl chains can be distinguished clearly. In contrast to the *trans* isomers, the *cis* isomers with both dodecyl and octadecyl chains form monolayers. The compound *cis* **9** displays the same packing as the octadecyl analogue in both solvents, with a change in the distance between equivalent points in abutting lamellae that corresponds to the difference in the alkyl chain length when compared with **8**.

These experiments allowed us to distinguish the *cis* and *trans* isomers of the octadecyl derivatives. The *trans* isomer forms two polymorphs. In all cases, the alkyl chains are revealed on the surface by STM, and adopt an extended all-*anti* conformation. Monolayers of the *cis* isomers **8** and **9** are readily observed at the liquid/solid interface upon deposition from both 1-octanol and 1-phenyloctane.

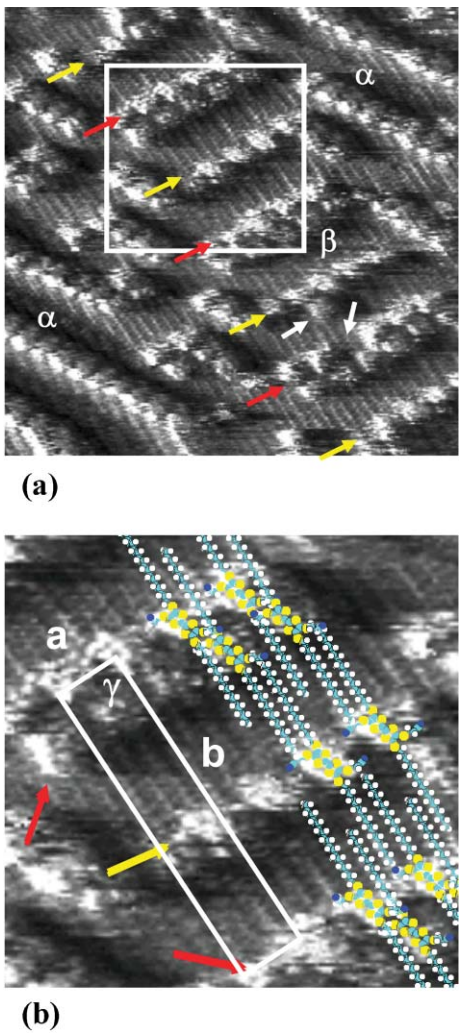

Fig. 5 (a) Large scale STM image of **6** monolayers. Two different polymorph domains, α and β, are indicated in the image. For the polymorph β, alternating double-core–single-core lamellae are indicated by red and yellow arrows, respectively. White arrows indicate a change in the packing as explained in the text. Image size is 19.5 × 19.5 nm; $I_t = 0.5$ nA, $V_t = -0.294$ V. (b) Zoom-in on the area indicated in (a). White arrows indicate two molecules forming a dimer. Red and yellow arrows indicate double-core and single-lamellae respectively. Nine molecules are superimposed on the image for clarity. Image size is 9 × 9 nm; $I_t = 0.5$ nA, $V_t = -0.294$ V.

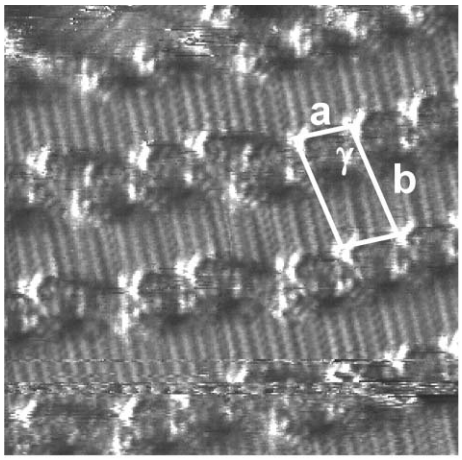

(a)

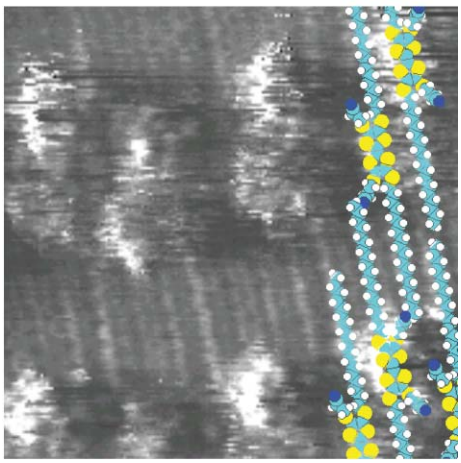

(b)

Fig. 6 (a) A monolayer of *cis*-isomer **8**. No single-core lamellae are observed, and the alkyl chains interdigitate. Image size is 13.8 × 13.8 nm; I_t = 0.9 nA, V_t = −0.31 V. (b) Monolayer of *cis*-isomer **8** with superimposed model molecules for clarity. Image size is 6 × 6 nm; I_t = 0.8 nA, V_t = −0.288 V.

However, the identification of isomers is not trivial, because the contrast of the TTF molecules is not a 'constant' and several different shapes are observed in the high tunnel current region which corresponds to the cores. One important factor here is the angle at which the tip passes across the central TTF unit, as we highlighted already for compound **4**, and as is shown in Fig. 7 for a monolayer of **8**. Depending on the orientation angle of the monolayer with respect to the scan direction (horizontal: from left to right) the contrast of the TTF groups and the alkyl chains changes, an effect which must therefore be attributed to a scanning artefact whose nature cannot be defined with certainty. Dramatically (depending on the scan direction), single bright uniform 'blobs' appear which actually consist of two TTF units, as revealed by the other images as well as being inferred by their size.

Compounds **10** and **11** in which the two alkyl chains are attached to the same "end" of the TTF moiety do not appear to adsorb readily at the graphite surface from either solvent, no image was ever obtained corresponding to the molecules,

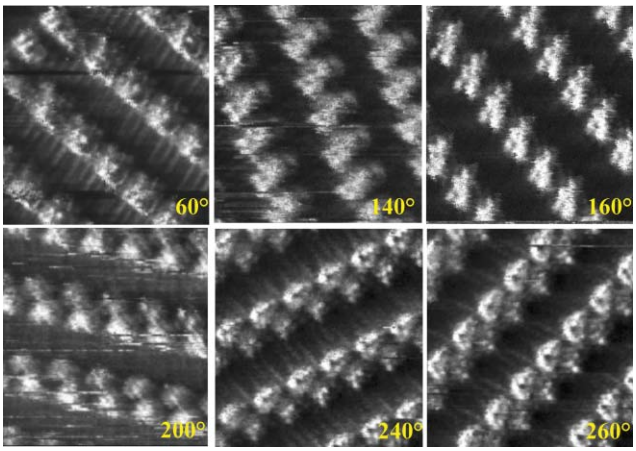

Fig. 7 A series of STM images of the *cis*-isomer **8** where the rotation angle of the scanning tip has been changed systematically. In the upper row, the dimer cores cannot be resolved; they appear as a single core. In the lower row, the dimer rows are clearly resolved as dimers. Image sizes *ca.* 9.6 × 9.6 nm. I_t = 0.3 nA, V_t = −0.175 V.

which are constitutional isomers of the pairs **6/8** and **7/9**. The reason for the lack of a favourable self-assembly process in this case is probably due to the difficulty of a stable alkyl chain packing on the surface and the ambivalence of the surface towards the propionitrile group (see the Conclusions section).

Four carboxylic acid derivatives were investigated; the dicarboxylic acid dialkyl chain derivatives **14** and **15** and the monocarboxylic acid dialkylchain derivatives **18** and **19**. For **14** and **15** only a few images were obtained at the liquid/solid interface, that were not of high resolution. The molecules appear to be organised in tapes, acting as dimers along the tape, as is shown for **15** in Fig. 8 for a monolayer formed from 1-octanol. For the monocarboxylic acid derivatives **18** and **19**, no monolayers were observed at the liquid/solid interface after deposition from either solvent, despite the possibility of

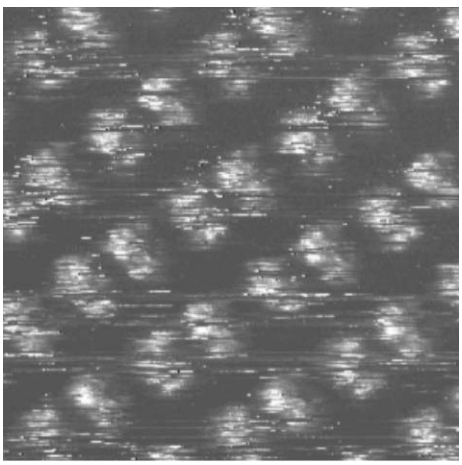

Fig. 8 STM image of the monolayer of **15** at the liquid/solid interface deposited from 1-octanol. The image is of poor quality, only the TTF moieties can be observed. The molecules appear to organise in tapes and appear as dimers along the long tape axis. Image size is 10.9 × 10.9 nm; I_t = 1.0 nA, V_t = −0.6 V.

formation of a hydrogen-bonded dimer through the carboxylic acid groups.[37] It appears that it is feasible for the dicarboxylic acids to form a head-to-tail type dimer which adsorbs on the surface (as seen in the STM images), but any head-to-head dimer—which could come about by hydrogen bonded dimers of the carboxylic acid groups—in the monosubstituted analogues is presumably unable to pack efficiently, since no evidence for monolayers was found.

The monoester **17** with two dodecyl chains (from both 1-phenyloctane and 1-octanol) and the diester **12** with two octadecyl chains (from 1-phenyloctane) form clearly different monolayers to the diacid **15**. The distance between two adjacent high tunnelling current areas for the diester **12** is 17.7 Å (*a* as indicated in Fig. 9) while the distance between adjacent rows is about 28 Å (*b* as indicated in Fig. 9).

This image contrasts strikingly with most of those obtained for monoester **17**, for which several polymorphous structures are observed (Fig. 10). In 1-phenyloctane, molecules of **17** align along a row and the alkyl chains are clearly visible. Note that these images reflect different polymorphs: the alkyl chains have a different orientation. In the α polymorph (Fig. 10a), the alkyl chain makes an angle with the stacking axis (*ca.* 44°), while for the β polymorph (Fig. 10b), the alkyl chains are almost perpendicular to the stacking axis of the molecules. The distance between two rows is 3.2 and 3.6 nm for the α and β polymorphs, respectively, and a very similar distance to that seen between lamella of compound **6**. The distance between the bright spots is about 0.95 nm for the α polymorph and 0.82 nm for the β polymorph, which is actually almost half the corresponding distance when compared with the diester **12**. This indicates that a bright area of tunnel current in the images for **12** probably contains two TTF groups. In 1-octanol different polymorphs are observed again: the δ and γ polymorphs (Fig. 10c–d, respectively) show characteristics reminiscent of the β polymorph of **6**.

Compounds **20** and **21**—in which the two alkyl chains are at one "end" of the molecule and hydrogen atoms are substituents in the remaining positions—did not organize into monolayers at the liquid/solid interface after deposition from either solvent. The presence of the ester groups in these compounds (**12** and **17**) seems to aid the formation of monolayers.

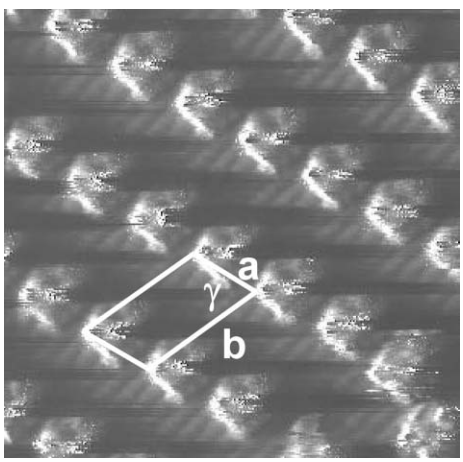

Fig. 9 STM image of **12** at the 1-phenyloctane/graphite interface; image size is 11.0 × 11.0 nm; I_t = 0.9 nA, V_t = −0.53 V.

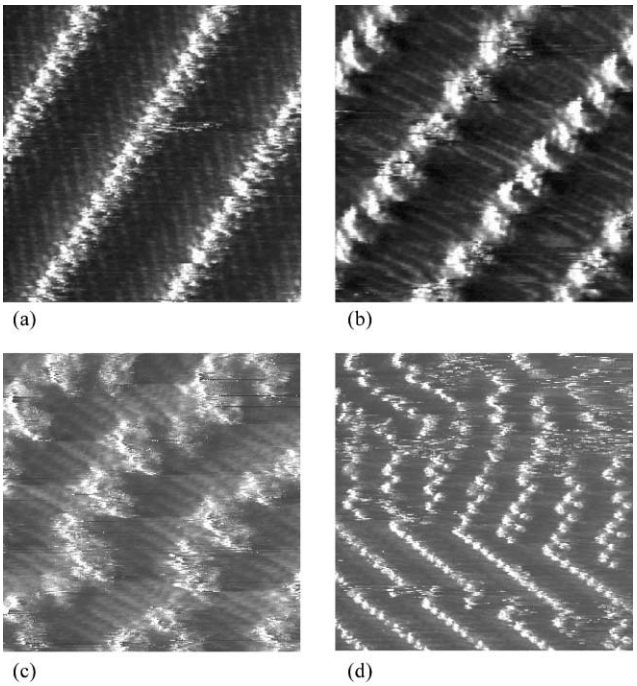

Fig. 10 STM images of the four polymorphous layers of **17** at the liquid/solid interface. In 1-phenyloctane: (a) image size is 10.7 × 10.7 nm; I_t = 0.6 nA, V_t = −0.354 V; (b) image size is 10.5 × 10.5 nm; I_t = 0.6 nA, V_t = −0.356 V. In 1-octanol: (c) image size is 10.9 × 10.9 nm; I_t = 0.8 nA, V_t = −0.39; (d) image size is 26.0 × 26.0 nm; I_t = 0.6 nA, V_t = −0.28 V.

Tetralkylated TTF derivatives. TTF derivatives **22**, **23** and **24** were investigated at the liquid/solid interface for three main reasons. First, it appeared from the experiments discussed above, that the presence of two alkyl chains at the same "end" of the TTF moiety hinders monolayer formation to some degree. Second, to test the self-assembly of molecules unable to have S···S side-on interactions in the monolayers. Third, should the monolayers form, the TTF cores would be essentially isolated from each other, giving the opportunity to study the properties of the π-electron rich aromatic on the graphite surface.

In either 1-octanol or 1-phenyloctane on the basal plane of graphite, these molecules all form self-assembled monolayers spontaneously at the liquid/solid interface, and identical patterns were observed in both solvents. The adsorption and scanning tunnelling spectroscopy (STS) measurements of **23** were presented in ref. 20, and to put these measurements in context we discuss here the STM experiments of all the tetraalkylated compounds in Chart 1, and support the hypotheses drawn from these results with molecular modelling simulations of the adsorption of **24** on graphite.

Fig. 11a–b are STM images of **24** at the liquid/solid interface. The molecules are organized in tapes where the TTF moieties are either adsorbed parallel (Fig. 11a) or at an angle (Fig. 11b) with respect to the tape direction. In both cases, the packing parameters are identical within experimental

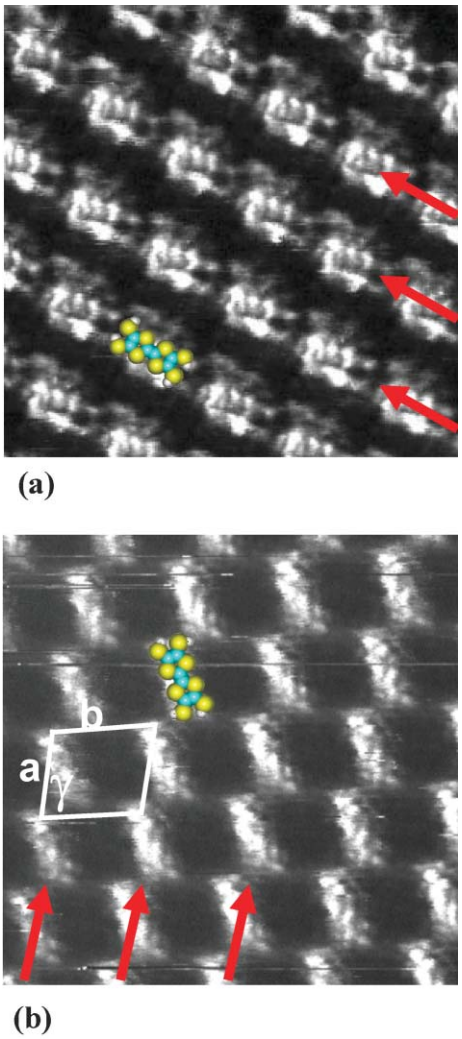

Fig. 11 STM images showing two different ordered layers of **24**. A TTF core model is superimposed on the patterns. Red arrows indicate the packing direction. (a) Image size is 10.1 × 10.1 nm; I_t = 0.4 nA, and V_t = −0.558 V. (b) Image size is 9.4 × 9.4 nm; I_t = 0.6 nA, and V_t = −0.19 V.

error: a = 17.5 ± 0.5 Å and b = 21.5 ± 0.7 Å. Alkyl chains could not be imaged. The variation in the TTF moiety contrast for the two observed polymorphs is most probably due to their different relative orientations with respect to the underlying graphite. This explanation is further supported with molecular modelling simulations (as will be discussed later).

Upon applying a drop of a solution of **23** in either 1-octanol or 1-phenyloctane, an ordered structure is spontaneously physisorbed at the liquid/solid interface, with the molecules organised in tapes. Fig. 12a shows an STM image of such a pattern. The intermolecular distance between two bright spots along a tape of **23** is a = 18.5 ± 0.4 Å (which is similar to that of **24**) and the distance between equivalent points in abutting tapes is b = 28.4 ± 0.6 Å. This increase in the inter-tape distance compared to **24** (21.5 ± 0.7 Å) is due to the increase in alkyl chain length (dodecyl chains for compound **24** and octadecyl chains for compound **23**). This observation supports the assumption that at least two alkyl chains per TTF moiety are fully adsorbed in the area between the tapes.

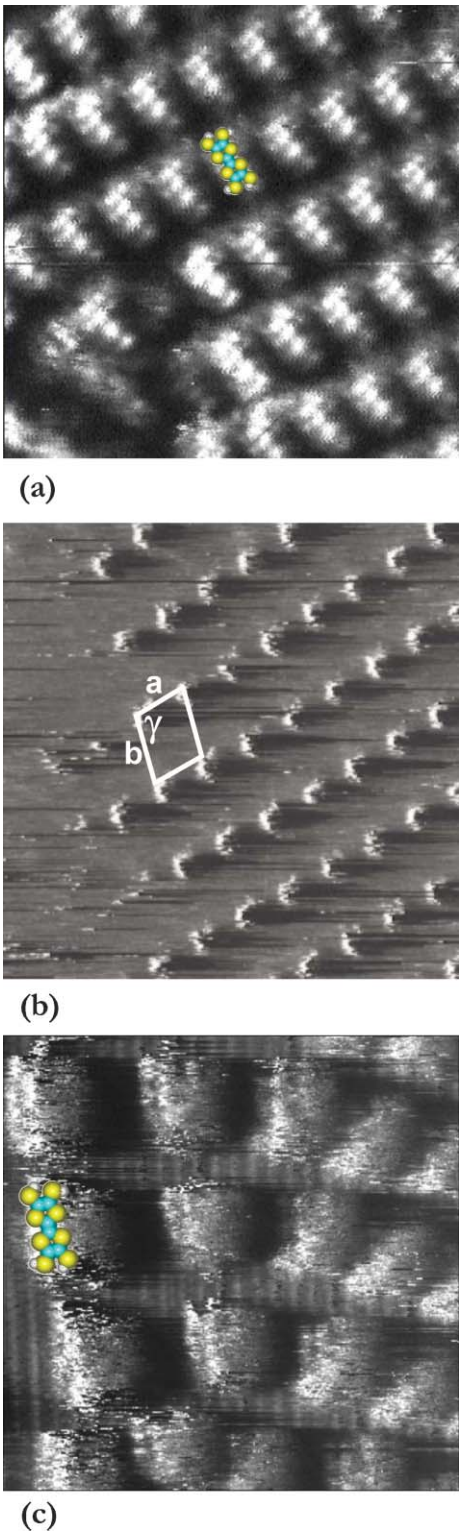

Fig. 12 STM images of patterns of **23** at the liquid/solid interface. Molecules are forming tapes, while the alkyl chains are adsorbed in between the tapes. (a) Image size is 13.6 × 13.6 nm; I_t = 0.4 nA, V_t = −0.92 V. A TTF core is superimposed on the pattern. (b) STM image of the 'loosely' packed ordering of **23** at the liquid/solid interface. Image size is 17.4 × 17.4 nm; I_t = 0.2 nA, V_t = −0.512 V. (c) STM image of a domain boundary between the closely packed monolayer (right) and the loosely packed monolayer (left) of **23**. A TTF core is superimposed on the pattern. Image size is 10.4 × 10.4 nm; I_t = 0.5 nA, V_t = −0.586 V.

Co-existing with the closely packed structure of **23** is a second polymorph. Fig. 12b shows an STM image of this polymorph at the liquid/solid interface. In this packing the repeat distance within a tape is 29.7 $\pm$ 0.9 Å. The distance between equivalent points in abutting tapes is 33.1 $\pm$ 1 Å. Fig. 12c shows an STM image of a domain boundary between a closely packed monolayer (right) and a loosely-packed layer (left). The orientation of the alkyl chains is unknown. While the proposed structure appears to be loosely-packed, it is consistent with the obtained STM data.

In most of the STM images of **23** the alkyl chains are not imaged, but very rarely they were. Fig. 13a is just such an STM-image. Though most likely the orientation of the alkyl chains and/or the TTF-cores is different from the polymorphs discussed above, the unit cell parameters are within experimental error identical to the pattern in Fig. 12a. Fig. 13b is a molecular model which reflects the ordering of the molecules in Fig. 13a. The tetraalkylated TTF molecule with $C_{22}H_{45}$ chains (**22**) also forms very well ordered monolayers in which the alkyl chains are observed more often. Fig. 13c–d show STM images of this compound at the 1-phenyloctane/graphite interface. Apparently, then, the probability of imaging the alkyl chains becomes higher the longer the alkyl chains. The distance between adjacent bright spots is about a = 18 Å and the distance between rows is on the order of b = 36 Å. The increase in this latter value is in line with the increased length of the alkyl chains. In those cases where alkyl chains are visible they are oriented almost perpendicular to the TTF rows, as in their stable configurations described in the molecular simulations below. The difficulty in observing the alkyl chains might be due either to the non-adsorption of one or more of the chains on the surface to allow for close packing or to the formation of multilayers, or both. Indeed, although the calculations indicate a stronger interaction between the TTF molecules and the graphite surface, once a monolayer is formed, it can act as a template for the adsorption of an additional layer of TTF molecules. In line with a recent report by Bai and coworkers operating under different conditions,[38] new experiments on **23** have revealed that TTF molecules might adsorb on top of the first monolayer. Fig. 14a shows an image where some TTF cores of **23** appear brighter at random places in the image, though always very close to TTF rows. This effect is attributed to the adsorption of two or more TTF cores on top of each other, as supported by the theoretical calculations. Bright spots also appear on top of the alkyl chains (Fig. 14b) in between TTF rows.

In addition, isolated bright spots appear from time to time (Fig. 15). No "interaction" with co-adsorbed TTF molecules

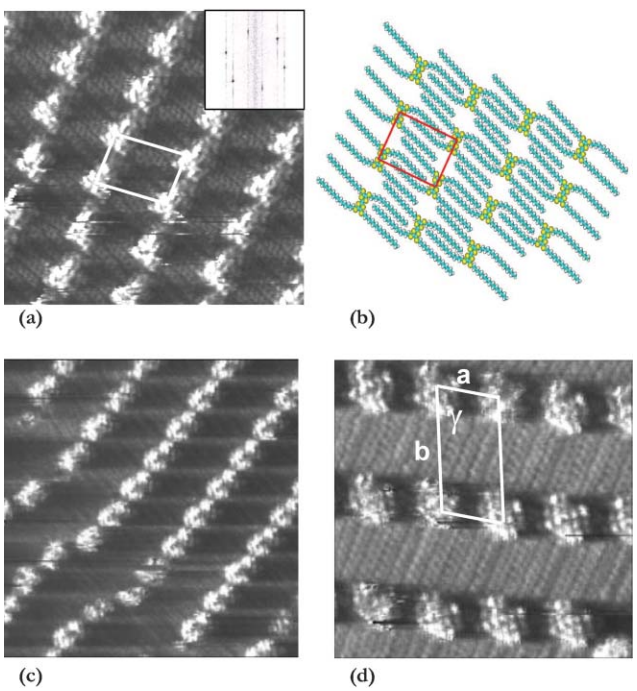

Fig. 13 STM images of **23** and **22** at the 1-phenyloctane/graphite interface. In these images, alkyl chains are clearly visible. (a) **23**: image size is 12 × 12 nm; I_t = 0.7 nA, V_t = −0.5 V Inset: FFT image of the underlying graphite surface. (b) Molecular model reflecting the ordering of **23**. (c) **22**: image size is 14.0 × 14.0 nm; I_t = 0.55 nA, V_t = −0.284 V. (d) **22**: image size is 8.4 × 8.4 nm; I_t = 0.7 nA, V_t = −0.270 V.

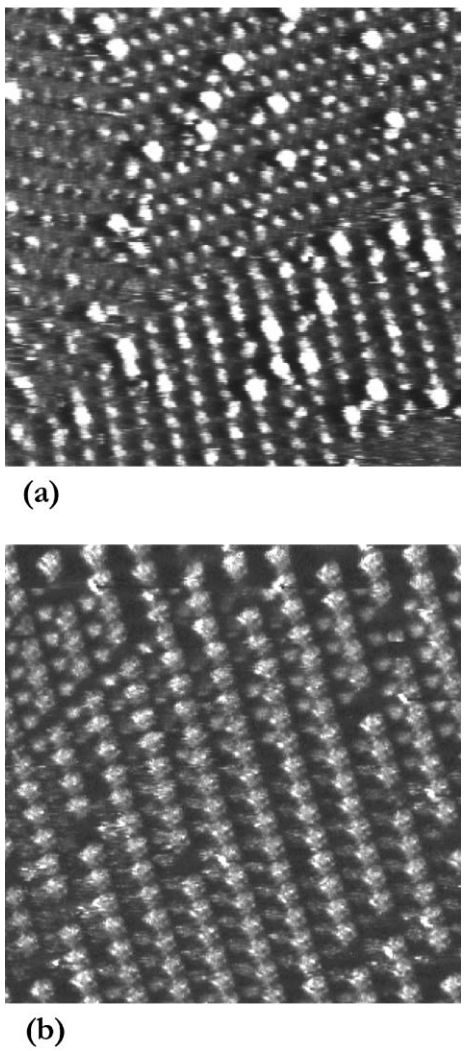

Fig. 14 STM images of **23** at the 1-phenyloctane graphite interface showing 'multi'-layer formation. (a) Image size is 50 × 50 nm; I_t = 0.5 nA, V_t = −0.85 V. (b) Image size is 30 × 30 nm; I_t = 0.4 nA, V_t = −0.90 V.

at the liquid/solid interface (at least not within the same layer) are possible here. One might notice some parallel lines of low contrast in the images. This effect could indicate that the arrangement of the isolated molecules is stabilized by the adsorption of solvent molecules. Note that the isolated structures of high brightness appear after a while measuring monolayers in the sessions, but do not appear immediately after applying the drop on the HOPG substrate.

In order to unravel the orientation of the tetraalkylated TTF derivatives with respect to the graphite surface, we have performed molecular mechanics calculations. We have considered the adsorption of **24** on a lattice of two planes of 20 × 20 graphite unit cells (see methodology below), as a model for the physisorption of tetraalkylated TTF derivatives.

The simulations provide three stable conformers (*i.e.*, three energy minima), those represented in Fig. 16. In all cases, the whole molecular backbone (TTF core and alkyl chains) is planar and parallel to the graphite surface, at an equilibrium distance of 3.5 Å with respect to the first underlying graphite plane. For the global minimum (defined as $\Delta E = 0$ kcal mol^{-1}, Fig. 16a), the TTF core is perfectly superimposed on two rings of the underlying graphite sheet (green dotted line); moreover, two of the four alkyl chains are commensurate with the graphite substrate (red dotted line) in a geometry known to be the epitaxial ordering of alkanes on graphite.[9a] In the second minimum (Fig. 16b), two alkyl chains are still commensurate with the underlying graphite lattice (red dotted line), whereas the TTF core no longer has a specific orientation with respect to the benzene rings of graphite. The difference in the total

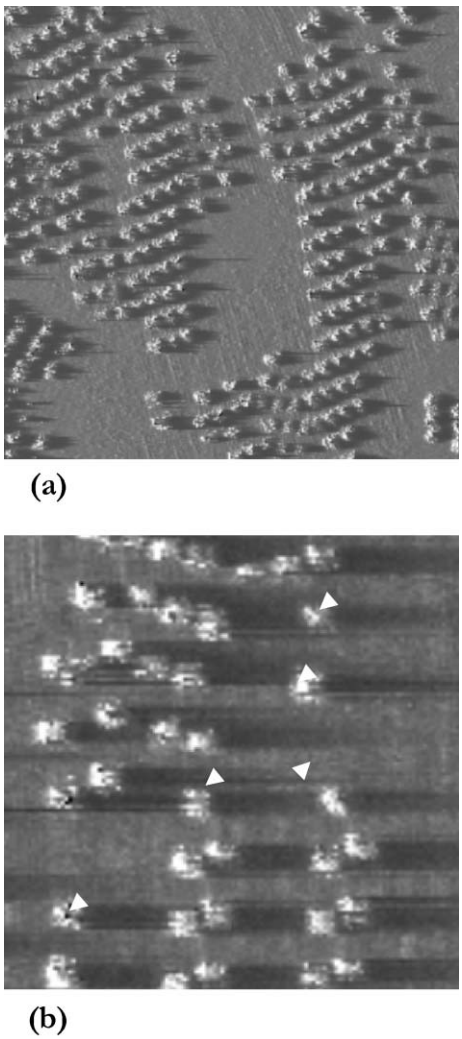

Fig. 15 STM images of **23** at the 1-phenyloctane graphite interface where the molecules appear isolated. White arrows indicate individually adsorbed molecules. (a) Image size is 55.0 × 55.0 nm; I_t = 0.5 nA, V_t = −0.372 V. (b) Image size is 23.1 × 23.1 nm; I_t = 0.5 nA, V_t = −0.298 V.

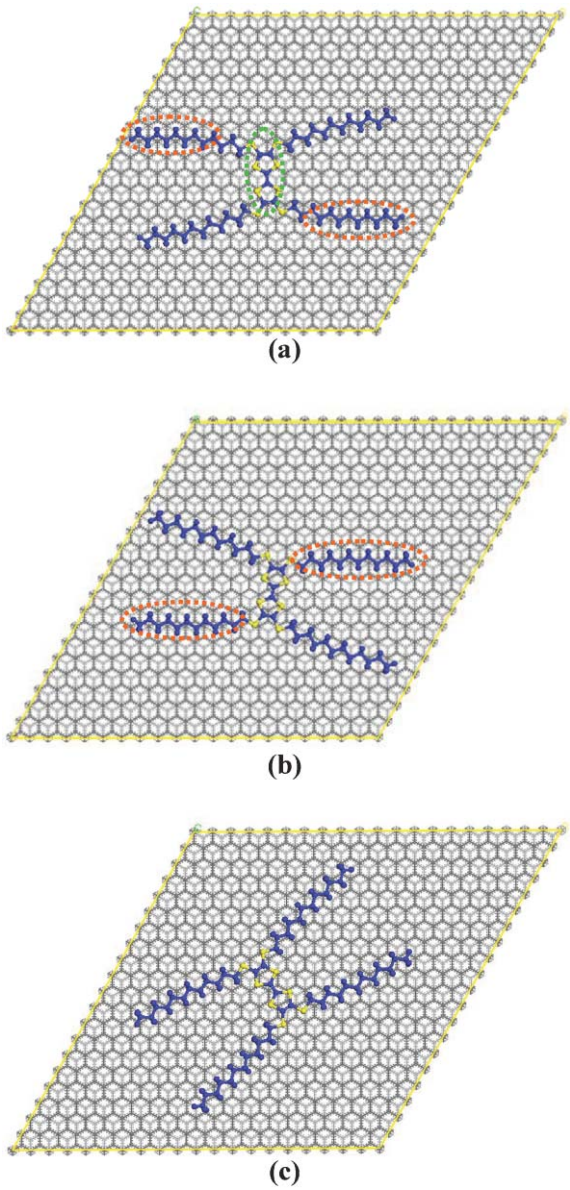

Fig. 16 Stable conformations of **24** on graphite. The yellow box represents the supercell used in the calculations. The first graphitic plane is coloured in dark grey, while the underlying plane appears in light grey (“line” representation). The molecule is displayed in blue, with the sulfur atoms represented in yellow (“ball and stick” representation). (a) Global minimum (defined as $\Delta E = 0$ kcal mol^{-1}); (b) and (c) local minima with $\Delta E = 0.63$ kcal mol^{-1} and $\Delta E = 1.27$ kcal mol^{-1}, respectively.

adsorption energy between the global minimum and this geometry amounts to 0.63 kcal mol^{-1}. In the less stable local minimum (Fig. 16c), we observe that both the alkyl chains and the TTF core have lost their specific orientation with respect to the underlying graphite lattice; ΔE in this case is estimated to be 1.27 kcal mol^{-1}.

These calculations show that the difference in adsorption energy among the different stable orientations of the molecules, with respect to the graphite substrate, is very small. Since the first molecules adsorbed on graphite are expected to dictate the pattern formation in 2D monolayers, these results are consistent with the polymorphism observed in the STM experiments (though our theoretical approach does not take into account either interactions between adjacent molecules or the solvent effects).

In order to further assess the possible formation of multilayers suggested by the STM experiments, molecular mechanics calculations were also carried out on stacks made of two **24** molecules. The stacking configurations were obtained from different starting geometries: the central carbon–carbon double bonds of the two molecules were rotated from a parallel configuration (0°) to a perpendicular configuration (90°) by steps of 10° (the distance between the molecules was allowed to relax during the simulations). This large set of starting configurations was chosen to ensure that the most stable conformers could be detected. The most stable stacking configuration is shown in Fig. 17. The equilibrium intermolecular distance (between TTF cores stacked along the Z axis) is estimated to be 3.8 Å, which is not an unreasonable value for π-stacks of this type of molecules.[39] This configuration differs from the fully cofacial one, by shifts along the X and the Y axes of 0.8 and 1.3 Å, respectively (Fig. 17a). This configuration results from a balance between the strong π–π interactions between the TTF cores and the steric hindrance between the hydrogen atoms of adjacent alkyl chains, which leads to an alternated configuration between alkyl chains in front of each other. Although the calculated binding energy between two TTF molecules (−96.1 kcal mol^{-1}) and between TTF and graphite (−136.9 kcal mol^{-1}) has no absolute meaning, the difference does show a preferential adsorption of **24** on graphite compared to the "adsorption" on another molecule. Once the formation of a 2-D monolayer is completed on graphite, further deposition of **24** is expected to form stacked layers of **24**.

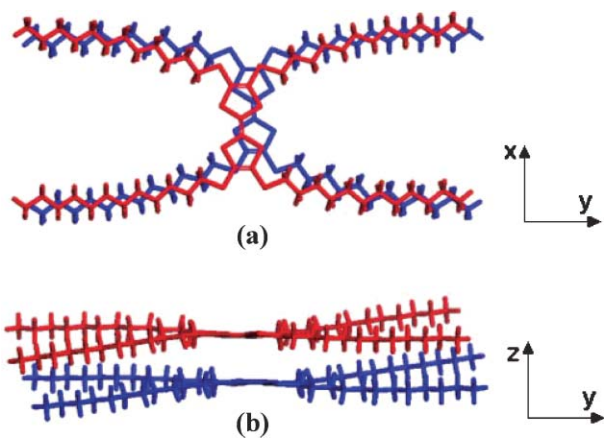

Fig. 17 Most stable configuration of a stack of two **24** molecules ("stick" representation). The TTF cores are shown from the top (a) and from a side view (b).

Overall, the ordering of tetraalkylated TTF molecules under these equilibrium conditions is rather complex. The formation of polymorphous patterns is in line with the molecular simulations, which point to several energetically favoured adsorption geometries. In addition, stacking of TTF molecules is not surprising giving their favourable π–π interactions.

Conclusions

Chemical control of the 2D packing of an important class of organic molecules, the tetrathiafulvalene derivatives, has been demonstrated. Upon changing the substituents and/or constitution of the molecule, different packing patterns are observed, from essentially isolated molecules, dimers, tapes, to a parquet-like arrangement and multilayers. Based upon the experimental observations, a number of empirically based conclusions can be drawn. (1) For the TTF derivatives with two or less alkyl chains, those compounds bearing two ester groups at one side of the TTF-core self-assemble at the graphite interface better than those with hydrogen atoms or thiopropionitrile groups, despite the potential of the CN group in organising molecules[40] these do not seem to aid in the organisation of the molecules presented here. (2) Dialkylated TTF derivatives give rise to physisorbed monolayers if they are at *trans* or *cis* positions of the central double bond, or if they are at the same side of the TTF core given that the substituent at the other side contains at least one ester group, or to a minor extent two carboxylic acid groups. (3) Tetraalkylated TTFs self-assemble at the liquid/solid interface with ease. To some extent, dipolar interactions might come into play. (4) In all cases where self-assembly is observed, the π-face of the TTF is practically parallel to the graphite surface.

The fact that for some TTF-derivatives self-assembled monolayers are not observed does not mean that their formation is impossible. It merely reflects the fact that under the given experimental conditions, which are similar for all compounds investigated, the TTF derivatives which were not observed to form adlayers are distinctly less prone to do so compared to the 'successful' derivatives. The distance between TTF moieties in the molecules varies with changing the packing pattern. Thus, the interaction between these units can be controlled at the liquid/solid interface. The side-on S···S interaction (which dominates in the 3D packing) pattern can be controlled in the observed 2D crystals. Herringbone, closely-packed lamellar, and loosely-packed lamellar structures were observed. Interestingly, adsorption of which appear to be individual molecules was observed for a tetraalkylated derivative.

The role of the solvents used in the experimental conditions used here is critical, giving rise to different lattice spacing in the two-dimensional crystals and to different stabilities of the monolayers. Despite the relative structural simplicity of these systems, their pattern formation is often surprising and counterintuitive. The results obtained here underline the importance of constitution on the self-assembly processes which lead to the formation of physisorbed monolayers.

Experimental

General details

The following products were purchased commercially (supplier as indicated) and were used without further purification: 1-bromododecane (Aldrich, 98%), 1-bromooctadecane (Aldrich), 1-bromodocosane (Aldrich, 96%). Thin-layer chromatography (TLC) was performed on aluminium plates coated with Merck Silica gel 60 F254. Developed plates were air-dried and scrutinized under a UV lamp. Silica gel 60 (35–70 mesh, SDS) was used for column chromatography. Melting points were determined by differential scanning calorimetry (DSC) using a Perkin Elmer DSC 7 instrument (discrete values) or a Melting Point SMP10, BIBBY Stuart Scientific instrument (intervals). LDI-TOF-MS were obtained using a Kratos Kompact Maldi 2 K-probe (Kratos Analytical) operating with pulsed extraction of the ions in linear high power mode. The samples were deposited directly onto a non-polished stainless steel sample plate from dichloromethane solution. ^{1}H and ^{13}C NMR spectra were recorded using the deuterated solvent as lock and tetramethylsilane as internal reference.

Synthesis of the known TTF derivatives discussed in this paper was carried out according to literature procedures: **1**,[24] **2**,[25] **3**,[26] **11**,[24] **21**,[33] and **23** and **24**[27] The synthetic procedures for the preparation of the remaining compounds are gathered in the electronic supplementary information.

STM experiments

Prior to imaging, all the TTF derivatives discussed in this paper (Chart 1) were dissolved in either 1-octanol (Aldrich, 99%) or 1-phenyloctane (Aldrich, 99%) at a concentration of approximately 1 mg per mL of solvent and a drop of either solution was applied on a freshly cleaved surface of highly oriented pyrolytic graphite (HOPG). The presented STM images were acquired in the variable current mode (constant height) under ambient conditions. In the STM images, white corresponds to the highest and black to the lowest measured tunnelling current. STM experiments were performed using a Discoverer scanning tunnelling microscope (Topometrix Inc., Santa Barbara, CA) with a typical frame acquisition time of 7 s, along with an external pulse/function generator (Model HP 8111 A), with negative sample bias. Tips were electrochemically etched from Pt/Ir wire (80/20%, diameter 0.2 mm) in a 2 N KOH–6 N NaCN solution in water. The experiments were repeated in several sessions using different tips to check for reproducibility and to avoid artefacts. Note that during the experiments, the STM tip is immersed in the supernatant solution. Different settings for the tunnelling current and the bias voltage were used, ranging from 0.3 to 1 nA and −10 to −1.5 V, respectively. All STM images contain raw data and are not subjected to any manipulation or image processing.

Molecular mechanics calculations

The adsorption of compound **24** on graphite has been simulated by Molecular Mechanics calculations. The graphite is simulated here by two planes of 20 × 20 unit cells (49.2 × 49.2 Å), which are repeated by using periodic lattice conditions. UFF (Universal Force Field),[41,42] which is used for all the optimizations described in this paper, has been validated in previous studies.[10a] In the simulations, the molecule is initially positioned far away from the graphite surface (about 6–7 Å), with the alkyl chains lying parallel to the substrate; the carbon atoms of the graphitic surface are frozen, since physisorption is not expected to alter the geometry of the substrate. The conformational search has been carried out starting from ten different conformations in which the angle between the molecular main axis and the graphite surface is varied from 0 to 90°. This sampling is performed in order to find the various energy minima associated to the physisorption process. The charge equilibration (QEq) algorithm has been used to equilibrate the charges in each fragment of the system, thus precluding possible charge-transfer processes at the interface. The geometry of the conjugated core of compound **24** has been initially optimized at the Density Functional Theory (DFT) level using the B3LYP functional and a 6–31g(d,p) basis set and has been frozen in the molecular mechanics simulations. The adsorption energy is defined as the total energy of the optimized system (molecule + substrate) minus the sum of the total energies of the separate fragments; only differences between the absolute values obtained were considered.

Acknowledgements

This work was supported by the DGI (Spain, Project BQU2003-00760), DGR (Catalonia, Project 2001SGR00362), the Belgian Government Federal Science Agency, through IUAP-V-03, the European Integrated Project NAIMO (NMP4-CT-2004-500355), and ESF SMARTON. E.G.-N. is grateful to the Generalitat de Catalunya for a predoctoral grant. S.D.F. thanks the Fund for Scientific Research-Flanders for financial support. The research is also supported by a working group from the COST program (D19/004/01). Research in Mons is partly supported by the European Commission, the Government of the Region of Wallonia (Phasing Out – Hainaut), and the Belgian National Fund for Scientific Research FNRS/FRFC. M.S. and V.L. acknowledge the F.R.I.A. for a doctoral fellowship. J.C. is Research Associate of the Belgian National Fund for Scientific Research (FNRS).

References

1 (*a*) J. S. Lindsey, *New J. Chem.*, 1991, **15**, 153–180; (*b*) D. Philp and J. F. Stoddart, *Angew. Chem., Int. Ed. Engl.*, 1996, **35**, 1155–1196; (*c*) D. S. Lawrence, T. Jiang and M. Levett, *Chem. Rev.*, 1995, **95**, 2229–2260; (*d*) A. Ulman, *Chem. Rev.*, 1996, **96**, 1533–1554; (*e*) L. M. Greig and D. Philp, *Chem. Soc. Rev.*, 2001, **30**, 287–302; (*f*) O. Ikkala and G. ten Brinke, *Chem. Commun.*, 2004, 2131–2137; (*g*) S. De Feyter and F. C. De Schryver, *J. Phys. Chem. B*, 2005, **109**, 4290–4302; (*h*) H. M. Keizer and R. P. Sijbesma, *Chem. Soc. Rev.*, 2005, **34**, 226–234 and references therein.

2 (*a*) *Nanotechnology*, ed. G. Timp, Springer-Verlag, New York, 1999. For recent articles, see: (*b*) A. Nojeh, G. W. Lakatos, S. Peng, K. Cho and R. F. W. Pease, *Nano Lett.*, 2003, **3**, 1187–1190; (*c*) L. Fu, L. C. Cao, Y. Q. Liu and D. B. Zhu, *Adv. Colloid Interface Sci.*, 2004, **111**, 133–157; (*d*) P. M. Mendes, A. H. Flood and J. F. Stoddart, *Appl. Phys. A*, 2005, **80**, 1197–1209; (*e*) J. Y. Ouyang, C. W. Chu, D. Sieves and Y. Yang, *Appl. Phys. Lett.*, 2005, **86**, 123507; (*f*) A. Vaseashta and J. Irudayaraj, *J. Optoelectron. Adv. Mater.*, 2005, **7**, 35–42; (*g*) A. A. Kornyshev, A. M. Kumetsov and J. Ulstrup,

ChemPhysChem, 2005, **6**, 583–586; (*h*) A. P. H. J. Schenning and E. W. Meijer, *Chem. Commun.*, 2005, 3245–3258.
3 (*a*) P. Packan, *Science*, 1999, **285**, 2079–2081; (*b*) C. Joachim, J. K. Gimzewski and A. Aviram, *Nature*, 2000, **408**, 541–548.
4 (*a*) G. A. Ozin, *Adv. Mater.*, 1992, **2**, 612–649; (*b*) R. D. Piner, J. Zhu, F. Xy, S. Hong and C. A. Mirkin, *Science*, 1999, **283**, 661–663; (*c*) S. Hong, J. Zhu and C. A. Mirkin, *Science*, 1999, **286**, 523–525; (*d*) R. Dagani, *Chem. Eng. News*, 2000, **16**, 25–32.
5 (*a*) C. P. Collier, G. Mattersteig, E. W. Wong, Y. Luo, K. Beverly, J. Sampaio, F. Raymo, J. F. Stoddart and J. R. Heath, *Science*, 2000, **289**, 1172–1175; (*b*) A. R. Pease, J. O. Jeppesen, J. F. Stoddart, Y. Luo, C. P. Collier and J. R. Heath, *Acc. Chem. Res.*, 2001, **34**, 433–444; (*c*) J. Chen, M. A. Reed, D. W. Price and J. M. Tour, *Appl. Phys. Lett.*, 2001, **78**, 3735–3737; (*d*) J. Chen, M. A. Reed, A. M. Rawlett and J. M. Tour, *Science*, 1999, **286**, 1550–1552; (*e*) R. L. Carroll and C. B. Gorman, *Angew. Chem., Int. Ed.*, 2002, **41**, 4378–4400; (*f*) R. M. Metzger, *Chem. Rev.*, 2003, **103**, 3803–3834; (*g*) P. Samori and J. P. Rabe, *J. Phys.: Condens. Matter*, 2002, **14**, 9955–9973; (*h*) G. Maruccio, R. Cingolani and R. Rinaldi, *J. Mater. Chem.*, 2004, **14**, 542–554.
6 (*a*) G. E. Poirier, *Chem. Rev.*, 1997, **97**, 1117–1127; (*b*) A. Ulman, *Acc. Chem. Res.*, 2001, **34**, 855–863 and references therein; (*c*) H. I. Kim, *Acc. Chem. Res.*, 2002, **35**, 547–553; (*d*) C. G. Zeng, B. Li, B. Wang, H. Q. Wang, K. D. Wang, Y. L. Yang, J. G. Hou and Q. S. Zhu, *J. Chem. Phys.*, 2002, **117**, 851–856.
7 (*a*) A. Ulman, *An Introduction to Ultrathin Organic Films*, Academic Press: San Diego, 1991; (*b*) F. Schreiber, *Prog. Surf. Sci.*, 2000, **65**, 151–256.
8 (*a*) J. Zhao and K. Uosaki, *Nano Lett.*, 2002, **2**, 137–140; (*b*) C. B. Gorman, R. L. Carroll and R. Fuierer, *Langmuir*, 2001, **17**, 6923–6930.
9 (*a*) J. P. Rabe and S. Buchholz, *Science*, 1991, **253**, 424–427; (*b*) L. C. Giancarlo and G. W. Flynn, *Annu. Rev. Phys. Chem.*, 1998, **49**, 297–336; (*c*) S. De Feyter, A. Gesquière, M. M. S. Abdel-Mottaleb, P. C. Grim, C. Meiners, M. Sieffert, S. Valiyaveettil, K. Müllen and F. C. De Schryver, *Acc. Chem. Res.*, 2000, **33**, 520–531; (*d*) P. Samorì, *J. Mater. Chem.*, 2004, **14**, 1353–1366.
10 (*a*) A. Gesquière, M. M. Abdel-Mottaleb, S. De Feyter, F. C. De Schryver, M. Sieffert, K. Müllen, A. Calderone, R. Lazzaroni and J.-L. Brédas, *Chem. Eur. J.*, 2000, **6**, 20, 3739–3746; (*b*) T. R. Baker, J. D. Mougous, A. Brackley and D. L. Patrick, *Langmuir*, 1999, **15**, 4884–4891; (*c*) F. Stevens and T. P. Beebe, *Langmuir*, 1999, **15**, 6884–6889; (*d*) J. V. Barth, T. Zambelli, J. Wintterlin, R. Schuster and G. Ertl, *Phys. Rev. B: Condens. Matter*, 1997, **55**, 12902–12905; (*e*) J. K. Gimzewski, C. Joachim, R. R. Schlittler, V. Langlais, H. Tang and I. Johannsen, *Science*, 1998, **281**, 531–533; (*f*) J. P. Rabe and S. Buchholz, *Phys. Rev. Lett.*, 1991, **66**, 2096–2099; (*g*) A. Stabel, R. Heinz, F. C. De Schryver and J. P. Rabe, *J. Phys. Chem.*, 1995, **99**, 505–507.
11 (*a*) M. M. S. Abdel-Mottaleb, N. Schuurmans, S. De Feyter, J. Van Esch, B. L. Feringa and F. C. De Schryver, *Chem. Commun.*, 2002, 1894–1895; (*b*) S. Hoeppener, J. Wonnemann, L. Chi, G. Erker and H. Fuchs, *ChemPhysChem*, 2003, **4**, 490–494; (*c*) S. Hoeppener, L. Chi and H. Fuchs, *ChemPhysChem*, 2003, **4**, 494–498.
12 (*a*) S. De Feyter and F. C. De Schryver, *Chem. Soc. Rev.*, 2003, **32**, 139–150; (*b*) S. De Feyter, M. Larsson, N. Schuurmans, B. Verkuijl, G. Zoriniants, A. Gesquière, M. M. Abdel-Mottaleb, J. van Esch, B. L. Feringa, J. van Stam and F. C. De Schryver, *Chem. Eur. J.*, 2003, **9**, 5, 1198–1205; (*c*) J. A. Theobald, N. S. Oxtoby, M. A. Philips, N. R. Champness and P. H. Beton, *Nature*, 2003, **424**, 1029–1031; (*d*) C. L. Claypool, F. Faglioni, W. A. Goddard, III and N. S. Lewis, *J. Phys. Chem. B*, 1999, **103**, 7077–7080; (*e*) X. Qiu, C. Wang, W. Zeng, B. Xu, S. Yin, H. Wang, S. Xu and C. Bai, *J. Am. Chem. Soc.*, 2000, **122**, 5550–5556; (*f*) X. Qiu, C. Wang, S. Yin, Q. Zeng, B. Xu and C. Bai, *J. Phys. Chem. B*, 2000, **104**, 3570–3574; (*g*) E. Mena-Osteritz and P. Bauerle, *Adv. Mater.*, 2001, **14**, 243–246; (*h*) A. Dmitriev, H. Spilmann, N. Lin, J. V. Barth and K. Kern, *Angew. Chem., Int. Ed.*, 2003, **42**, 2670–2673; (*i*) P. Samori, N. Severin, C. D. Simpson, K. Müllen and J. P. Rabe, *J. Am. Chem. Soc.*, 2002, **124**, 9454–9457.
13 (*a*) C. Messerschmidt, A. Schulz, J. P. Rabe, A. Simon, O. Marti and J.-H. Fuhrhop, *Langmuir*, 2000, **16**, 1299–1305; (*b*) X. Du and V. Hlady, *J. Phys. Chem. B*, 2002, **106**, 7295–7299; (*c*) J. Yin, Q. Guo, R. E. Palmer, N. Campos and J. K. M. Sanders, *J. Phys. Chem. B*, 2003, **107**, 209–216; (*d*) J. J. Garcia-Lopez, S. Zapotoczny, P. Timmermen, F. C. J. M. van Veggel, J. Vancso, M. Crego-Calama and D. N. Reinhoudt, *Chem. Commun.*, 2003, 352–353.
14 (*a*) M. E. Stawasz, D. L. Sampson and B. A. Parkinson, *Langmuir*, 2000, **16**, 2326; (*b*) Y. Kaneda, M. E. Stawasz, D. L. Sampson and B. A. Parkinson, *Langmuir*, 2001, **17**, 6185–6195; (*c*) P. Wu, Q. D. Zeng, S. D. Xu, C. Wang, S. X. Yin and C. L. Bai, *ChemPhysChem*, 2001, **2**, 750–754.
15 (*a*) M. B. Nielsen, C. Lomholt and J. Becher, *Chem. Soc. Rev.*, 2000, **29**, 153–164; (*b*) J. L. Segura and N. Martín, *Angew. Chem., Int. Ed.*, 2001, **40**, 1372–1409.
16 (*a*) M. R. J. Bryce, *Chem. Soc. Rev.*, 1991, **20**, 355–390; (*b*) N. S. Nalwa, *Handbook of Organic Conductive Molecules and Polymers, vol. 1*, John Wiley & Sons, New York, 1997.
17 M. Mas-Torrent, P. Hadley, S. T. Bromley, X. Ribas, J. Tarres, M. Mas, E. Molins, J. Veciana and C. Rovira, *J. Am. Chem. Soc.*, 2004, **126**, 8546–8553.
18 (*a*) T. Sleator and T. Tycko, *Phys. Rev. Lett.*, 1998, **60**, 1418–1421; (*b*) S. N. Magonov and M.-H. Whangbo, *Adv. Mater.*, 1994, **6**, 355–371; (*c*) N. A. Kato, M. Hara, H. Sasabe and W. Knoll, *Nanotechnology*, 1996, **7**, 122–127; (*d*) S. N. Maganov, G. Bar, E. Séller, E. B. Yagubskii, E.E. Laukhina and H.-J. Cantow, *Ultramicroscopy*, 1992, **42–44**, 1009; (*e*) N. Ara-Kato, K. Yase, H. Shigekawa, M. Yoshimura and A. Kawazu, *Synth. Met.*, 1995, **70**, 1245–1246; (*f*) J. A. Last, A. C. Hillier, D. E. Hooks, J. B. Masón and M. D. Ward, *Chem. Mater.*, 1998, **10**, 422–437; (*g*) Z. Z. Wang, J. C. Girard, C. Pasquier, D. Jérome and K. Bechgaard, *Phys. Rev. B: Condens. Matter*, 2003, **67**, 121401(R).
19 E. Gomar-Nadal, M. M. S. Abdel-Mottaleb, S. De Feyter, J. Veciana, C. Rovira, D. B. Amabilino and F. C. De Schryver, *Chem. Commun.*, 2003, 906–907.
20 M. M. S. Abdel-Mottaleb, E. Gomar-Nadal, S. De Feyter, M. Zdanowska, J. Veciana, C. Rovira, D. B. Amabilino and F. C. De Schryver, *Nano Lett.*, 2003, **3**, 1375–1378.
21 J. J. Novoa, M. C. Rovira, C. Rovira, J. Veciana and J. Tarrés, *Adv. Mater.*, 1995, **7**, 233.
22 (*a*) S. A. Shikin, T. S. Berzina, P. S. Sotnikov, V. I. Troitsky, O. Y. Nielands, G. G. Pukitis and V. Y. Khodorkovsky, *Biol. Membr.*, 1990, **7**, 1111–1117; (*b*) T. S. Berzina, V. I. Troitsky and L. G. Yanusova, *Biol. Membr.*, 1990, **7**, 1165–1172; (*c*) K. Naito, A. Miura and M. Azuma, *J. Am. Chem. Soc.*, 1991, **113**, 6386–6395; (*d*) A. S. Dhindsa, Y.-P. Song, J. P. Badyal, M. R. Bryce, Y. M. Lvov, M. C. Petty and J. Yarwood, *Chem. Mater.*, 1992, **4**, 724–728; (*e*) C. M. Yip and M. D. Ward, *Langmuir*, 1994, **10**, 549–556; (*f*) P. Cea, C. Lafuente, J. S. Urieta, M. C. López and F. M. Royo, *Langmuir*, 1997, **13**, 4892–4897; (*g*) Y. Urai, C. Ohe and K. Itoh, *Langmuir*, 1998, **14**, 4873–4879; (*h*) R. Yuge, A. Miyazaki, T. Enoki, K. Tamada, F. Nakamura and M. Hara, *J. Phys. Chem. B*, 2002, **106**, 6894–6901; (*i*) T. Akutagawa, M. Uchigata, T. Hasegawa, T. Nakamura, K. A. Nielsen, J. O. Jeppesen, T. Brimert and J. Becher, *J. Phys. Chem. B*, 2003, **107**, 13929–13938; (*j*) M. A. Herranz, L. Yu, N. Martín and L. Echegoyen, *J. Org. Chem.*, 2003, **68**, 8379–8385; (*k*) H. Miyata, Y. Tatewaki, T. Akutagawa, T. Hasegawa, T. Nakamura, C. C. Christensen and J. Becher, *Thin Solid Films*, 2003, **438–439**, 1–6; (*l*) C. Jia, D. Zhang, Y. Xu, W. Xu and D. Zhu, *Synth. Met.*, 2003, **137**, 979–980; (*m*) E. Dahlstedt, J. Hellberg, R. M. Petoral, Jr. and K. Uvdal, *J. Mater. Chem.*, 2004, **14**, 81–85.
23 (*a*) D. M. Cyr, B. Venkataraman and G. W. Flynn, *Chem. Mater.*, 1996, **8**, 1600–1615; (*b*) C. L. Claypool, F. Faglioni, W. A. Goddard, III, H. B. Gray, N. S. Lewis and R. A. Marcus, *J. Phys. Chem. B*, 1997, **101**, 5978–5995.
24 K. B. Simonsen, N. Svenstrup, J. Lau, O. Simonsen, P. Mork, G. J. Kristensen and J. Becher, *Synthesis*, 1996, 407–418.
25 C. U. Pittman, Jr., M. Narita and Y. F. Liang, *J. Org. Chem.*, 1976, **41**, 2855–2860.
26 N. Svenstrup, K. M. Rasmussen, T. K. Hansen and J. Becher, *Synthesis*, 1994, 809–812.
27 P. Wu, G. Saito, K. Imaeda, Z. Shi, T. Mori, T. Enoki and H. Inokuchi, *Chem. Lett.*, 1986, 441–444.
28 (*a*) G. Steimecke, R. Kirmse and E. Hoyer, *Z. Chem.*, 1975, **15**, 28–29; (*b*) G. Steimeche, H.-J. Sieler, R. Kirmse and E. Hoyer,

Phosphorus, Sulfur Relat. Elem., 1979, **7**, 49–55; (*c*) R.-M. Olk, B. Olk, W. Dietzsch, R. Kirmse and E. Hoyer, *Coord. Chem. Rev.*, 1992, **117**, 99–131; (*d*) T. K. Hansen, J. Becher, T. Jørgensen, K. S. Varma, R. Khedekar and M. P. Cava, *Org. Synth.*, 1996, **73**, 270–277.
29 P. R. Prag, J. D. Kilburn, M. C. Petty, C. Pearson and T. G. Ryan, *Synthesis*, 1994, 613–618.
30 (*a*) E. Fanghänel, L. van Hinh, G. Schukat and J. Patzsch, *J. Prakt. Chem.*, 1989, **331**, 479–485; (*b*) M. Salle, A. Gorgues, M. Jubault, K. Boubekeur and P. Batail, *Tetrahedron*, 1992, **48**, 3081–3090; (*c*) M. Formigué, C. E. Uzelmeier, K. Boubekeur, S. L. Bartley and K. R. Dunbar, *J. Organomet. Chem.*, 1997, **529**, 343–350; (*d*) R. Ballardini, V. Balzani, J. Becher, A. Di Fabio, M. T. Gandolfi, G. Mattersteig, M. B. Nielsen, F. M. Raymo, S. J. Rowan, J. F. Stoddart, A. J. P. White and D. J. Williams, *J. Org. Chem.*, 2000, **65**, 4120–4126.
31 A. Souizi, A. Robert, P. Batail and L. Ouahab, *J. Org. Chem.*, 1987, **52**, 1610–1611.
32 M. Vandevyver, M. Roulliay, J. P. Bourgoin, A. Barraud, V. Gionis, V. C. Kakoussis, G. A. Mousdis, J.-P. Morand and O. Noel, *J. Phys. Chem.*, 1991, **95**, 246–251.
33 M. González, N. Martín and J. L. Segura, *Tetrahedron Lett.*, 1998, **39**, 3269–3272.
34 (*a*) S. Hünig and H. Berneth, *Top. Curr. Chem.*, 1980, **92**, 1–44; (*b*) S. Sakura, H. Imai, H. Anzai and T. Moriya, *Bull. Chem. Soc. Jpn.*, 1988, **61**, 3181–3186; (*c*) D. L. Lichtenberger, R. L. Johnston, K. Hinkelmann, T. Suzuki and F. Wudl, *J. Am. Chem. Soc.*, 1990, **112**, 3302–3307; (*d*) M. Salle, M. Jubault, A. Gorgues, K. Boubekeur, M. Fourmigue, P. Batail and E. Canadell, *Chem. Mater.*, 1993, **5**, 1196–1198; (*e*) M. Salle, A. J. Moore, M. R. Bryce and M. Jubault, *Tetrahedron Lett.*, 1993, **34**, 7475–7478; (*f*) C. Rovira, J. Veciana, N. Santal, J. Tarres, J. Cirujeda, E. Molins, J. Llorca and E. Espinosa, *J. Org. Chem.*, 1994, **59**, 3307–3313; (*g*) A. S. Batsanov, M. R. Bryce, J. N. Heaton, A. J. Moore, P. J. Skabara, J. A. K. Howard, E. Orti, P. M. Viruela and R. Viruela, *J. Mater. Chem.*, 1995, **5**, 1689–1696; (*h*) E. Ribera, J. Veciana, E. Molins, I. Mata, K. Wurst and C. Rovira, *Eur. J. Org. Chem.*, 2000, 2867–2875.
35 The cyclic voltammetry of compounds with very long alkyl chains can give rise to irreversible processes, although the dodecyl derivatives are well-behaved. See: P. Cea, J. I. Pardo, J. S. Urieta, M. C. Lopez and F. M. Royo, *Electrochim. Acta*, 2000, **46**, 589–597.
36 (*a*) G. Saito, T. Teramoto, A. Otsuka, Y. Sugita, T. Ban, M. Kusunoki and K.-I. Sakaguchi, *Synth. Met.*, 1994, **64**, 359–368; (*b*) J. Llacay, J. Tarrés, C. Rovira, J. Veciana, M. Mas and E. Molins, *J. Phys. Chem. Solids*, 1997, **58**, 1675–1678; (*c*) D. V. Konarev, E. F. Valeev, Yu. L. Slovokhotov, Yu. M. Shul'ga, O. S. Roschupkina and R. N. Lyubovskaya, *Synth. Met.*, 1997, **88**, 85–87; (*d*) D. V. Konarev, A.Yu. Kovalevsky, P. Coppens and R. N. Lyubovskaya, *Chem. Commun.*, 2000, 2357–2358; (*e*) D. V. Konarev, R. N. Lyubovskaya, N. V. Drichko, E. I. Yudanova, Y. M. Shul'ga, A. L. Litvinov, V. N. Semkin and B. P. Tarasov, *J. Mater. Chem.*, 2000, **10**, 803–818; (*f*) D. V. Konarev, I. S. Neretin, Y. L. Slovokhotov, A. L. Litvinov, A. Otsuka, R. N. Lyubovskaya and G. N. Saito, *Synth. Met.*, 2002, **131**, 87–92.
37 D. Hadži and S. Detoni, in *The Chemistry of Acid Derivatives, Part 1*, ed. S. Patai, J. Wiley & Sons, New York, 1992.
38 STM measurements of **23** under (presumably) dry conditions revealed apparent stacks: J. Lu, Q.-d. Zeng, C. Wang, L.-J. Wan and C.-L. Bai, *Chem. Lett.*, 2003, **32**, 856–857.
39 (*a*) A. Janiak, *J. Chem. Soc., Dalton Trans.*, 2000, 3885–3896; (*b*) C. A. Hunter, K. R. Lawson, J. Perkins and C. J. Urch, *J. Chem. Soc., Perkin Trans. 2*, 2001, 651–669; (*c*) G. Lincke, *Dyes Pigm.*, 2003, **59**, 1–24.
40 T. Yokoyama, S. Yokoyama, T. Kamikado, Y. Okuno and S. Mashiko, *Nature*, 2001, **413**, 619–621.
41 A. K. Rappé, C. J. Casewit, K. S. Colwell, W. A. Goddard, III and W. M. Skiff, *J. Am. Chem. Soc.*, 1992, **114**, 10024–10035.
42 C. J. Casewit, K. S. Coldwell and A. K. Rappé, *J. Am. Chem. Soc.*, 1992, **114**, 10035–10046.